Biodistribution and Blood Metabolism of 1-^{11}C-Methyl-4-Piperidinyl n-Butyrate in Humans: An Imaging Agent for In Vivo Assessment of Butyrylcholinesterase Activity with PET

Anne Roivainen, PhD[1]; Juha Rinne, MD, PhD[1]; Jere Virta, BM[1]; Tarja Järvenpää, MD[1]; Satu Salomäki, MSc[1]; Miexiang Yu, PhD[2]; and Kjell Någren, PhD[2]

[1]Turku PET Centre, Turku University Hospital, Turku, Finland; and [2]Radiopharmaceutical Chemistry Laboratory, University of Turku, Turku, Finland

1-^{11}C-Methyl-4-piperidinyl n-butyrate (^{11}C-MP4B) is a new radiopharmaceutical for the in vivo assessment of butyrylcholinesterase (BuChE) activity using PET. To quantify in vivo activity of BuChE with a kinetic model, investigators must determine the time course of radioactivity associated with unchanged ^{11}C-MP4B. We aimed at clarifying the metabolic fate and whole-body distribution of intravenously administered ^{11}C-MP4B in man. **Methods:** High-performance liquid chromatography and thin-layer chromatography assays were performed to determine the amounts of intact ^{11}C-MP4B and its radioactive hydrolysis product in blood withdrawn during PET. In addition, we evaluated the distribution and kinetics of ^{11}C-MP4B uptake in human brain and main organs. **Results:** The analysis of plasma samples of 28 human subjects (10 patients with Alzheimer's disease [AD] and 18 healthy controls) showed that the level of unmetabolized ^{11}C-MP4B decreases rapidly from 28% ± 14% (mean ± SD) at 0.5 min to 7% ± 6% at 15 min after injection. Large individual variation was observed in the rate of plasma ^{11}C-MP4B hydrolysis, but no significant differences were found in the degradation of ^{11}C-MP4B either between male and female or between healthy subjects and patients. The whole-body distribution of ^{11}C-MP4B showed the highest activities in the urinary bladder, renal pelvis, stomach, salivary glands, liver, kidneys, spleen, vertebral column, and brain. In patients with AD, ^{11}C-MP4B activity in the brain was highest in cerebellum, followed by striatum, pons, and thalamus. Lower ^{11}C-MP4B activity was seen in cortical areas. **Conclusion:** Our results indicate that ^{11}C-MP4B is excreted rapidly through the renal system. Careful analysis of plasma metabolites is required to determine the accurate arterial input function for quantitative PET measurement. Biodistribution of ^{11}C-MP4B in the brains of patients with AD appears to be in accordance with the distribution of BuChE seen in postmortem studies of human brain, except for the observed higher activity in striatum than in cortex. Further studies of the cerebral distribution and regional kinetic analysis of ^{11}C-MP4B are in progress.

Received Apr. 21, 2004; revision accepted Jul. 21, 2004.

For correspondence or reprints contact: Anne Roivainen, PhD, Turku PET Centre, Turku University Hospital, P.O. Box 52, FI-20521 Turku, Finland.

E-mail: anne.roivainen@pet.tyks.fi

Key Words: butyrylcholinesterate; Alzheimer's disease; PET

J Nucl Med 2004; 45:2032–2039

Deficits in cholinergic function contribute to the pathology of Alzheimer's disease (AD) and other dementing diseases, such as dementia with Lewy bodies and Parkinson's disease, that affect cognition, behavior, and activities of daily living. Pharmacologic interventions directed toward these deficits are based on acetylcholinesterase (AChE) inhibition. Acetylcholine, a brain neurotransmitter, is basically degraded by 2 enzymes, AChE and butyrylcholinesterase (BuChE), leading to termination of cholinergic neurotransmission. Until recently, the role of BuChE has been largely ignored. However, increasing evidence supports the role of BuChE in the pathophysiology of AD. In severe AD, the level of AChE is decreased by as much as 90% compared with normal values, whereas the level of BuChE increases by approximately 30% (*1–3*). In such cases, BuChE may be a more appropriate therapeutic target. Indeed, selective BuChE inhibitors in rodents have increased acetylcholine concentration and improved learning and memory (*4*). BuChE is expressed in the brain together with AChE. In the brains of patients with AD, BuChE is highly concentrated in and around the vessels with amyloid angiopathy and senile plaques along with β-amyloid (*2,5*).

PET can be applied to detect cholinergic deficits at an early stage of a dementing disease and also to study the effect of ChE inhibitors or other cholinergic drugs in vivo (*6–9*). *N*-methylpiperidinyl esters have been extensively characterized as synthetic substrates for AChE (*7,10–12*). 1-^{11}C-Methyl-4-piperidinyl acetate (^{11}C-MP4A) and 1-^{11}C-methyl-4-piperidinyl propionate (^{11}C-MP4P) are already in clinical use for in vivo assessment of AChE activity associated with AD using PET (*13–15*). 1-^{11}C-

Methyl-4-piperidinyl n-butyrate (^{11}C-MP4B), a substrate for BuChE but not for AChE, is a new radiopharmaceutical for the in vivo assessment of BuChE activity using PET (*16*). In the present study, we evaluated the biodistribution and blood metabolism of ^{11}C-MP4B in healthy volunteers and patients with AD.

MATERIALS AND METHODS

Chemicals and Reagents

Tetraisopropyl pyrophosphoramide (iso-OMPA) and BuChE (EC 3.1.1.8, from horse serum) were purchased from Sigma. 4-Butyryl-piperidine hydrochloride and 1-methyl-4-butyryl-piperidine hydrochloride were obtained from ABX Advanced Biochemical Compounds. Sterile solvents used in the ^{11}C-MP4B formulation were obtained from the Pharmacy of Turku University Hospital. Other chemicals were obtained from commercial sources and were of analytic grade.

Preparation of ^{11}C-MP4B

^{11}C-MP4B was produced by the reaction of 4-butyryl-piperidine, generated in situ from its hydrochloride salt using 1,2,2,6,6-pentamethyl-piperidine (PMP), and ^{11}C-methyl triflate in methanol–acetonitrile for 1 min at 60°C. The crude product was purified using high-performance liquid chromatography (HPLC) with a μPorasil column (Waters). After addition of 0.3 mL of sterile propylene glycol–ethanol (7:3 v/v) and 100 μL of 0.1 mol/L HCl, the fraction containing the product was evaporated and redissolved in physiologic phosphate buffer (0.1 mol/L, pH 7.4) and filtered through a 0.2-μm Gelman Acrodisc 4192 sterile filter.

Quality control was performed using HPLC with a Waters μ-Bondapak C18 10 μ, 3.9 × 300 mm column (Waters) and a gradient of phosphoric acid (50 mmol/L) and acetonitrile. A reference material of MP4B was coinjected with the product and the chemical identity of the product was verified by coelution of the main ultraviolet-absorbing component with the response of the radioactivity detector. The k′ of ^{11}C-MP4B in the analysis system was 1.7.

Subjects

A healthy 22-y-old male volunteer was recruited for whole-body PET of ^{11}C-MP4B distribution. Twenty-eight subjects (10 patients with AD and 18 healthy controls) were studied for the blood metabolism and distribution and biokinetics of ^{11}C-MP4B in the brain. Of the subjects, 18 were female and 10 male, and their mean age was 67 ± 6 y (range, 58–80 y). The studies were reviewed and approved by the Joint Committee on Ethics of the Turku University and the Turku University Hospital and by the National Agency of Medicine. All the subjects gave their written informed consent before participating in this study.

Whole-Body Distribution of ^{11}C-MP4B

Whole-body PET was performed on a healthy volunteer using an Advance PET scanner (General Electric Medical Systems) operated in 2-dimensional mode. The imaging field of view in axial length was 15.2 cm. Imaging was performed with the patient in the supine position and arms alongside the body. Data acquisition started 10 min after an intravenous bolus injection of 725 MBq of ^{11}C-MP4B, proceeding from the head to the pelvic floor, excluding legs. Six bed positions were required for this measurement, with a 5-min acquisition time for each position. The acquired data were iteratively reconstructed with attenuation correction using the ordered-subsets expectation maximization (OSEM) algorithm. Quantification of tracer uptake was performed by standard region-of-interest (ROI) analysis, followed by the calculation of standardized uptake value (SUV). For each organ, circular ROIs with fixed diameter of 3.0 mm (14 pixels) were drawn and averaged on 3 coronal slices.

The subject was asked to void immediately before ^{11}C-MP4B injection. After completion of PET, the total activity in the whole urine volume was determined within 50 min after the tracer administration. A urine sample of 2.5 mL was measured with a well-type γ-counter (7.62 × 7.62 cm [3 × 3 in.]; Bicron) cross-calibrated with a dose calibrator (VDC-404; Veenstra Instruments), and the fraction of injected dose (%) excreted in the urine was calculated.

Dynamic PET of Brain Area

PET was performed on the patients and healthy controls using an Advance PET scanner operated in 3D mode. Two catheters were inserted: in an anterior cubital vein for the injection of ^{11}C-MP4B and in the opposite radial artery for the blood sampling. Transmission scanning for attenuation correction was performed before each emission scan. For dynamic PET, the subjects were intravenously injected with 703 ± 63 MBq of ^{11}C-MP4B (range, 576–805 MBq) as a bolus during 80 s and promptly flushed with saline after injection. The data acquisition started at the beginning of injection (1 × 30 s, 4 × 15 s, 5 × 30 s, 2 × 60 s, 2 × 120 s, 6 × 300 s, and 2 × 600 s frames), with 60-min total duration.

All image acquisition data were corrected for dead time, decay, and measured photon attenuation and were iteratively reconstructed with the OSEM algorithm. ROIs were selected to represent the areas of cerebellum, striatum, and cortex, and the radioactivities (kBq/mL) for ROIs were computed.

Blood Sampling During PET

To obtain the input function, arterial radioactivity concentrations were measured using an automated device (Fluid Radioactivity Quantifier; General Electric Medical Systems) for the first 10 min after injection, thus covering the time of peak radioactivity in blood. Manual sampling was used for the remainder of the study, and the radioactivity was measured with an automatic γ-counter (1480 Wizard 3″; EG&G Wallac). In addition, arterial blood samples were obtained at 0.5, 1, 1.5, 3, 5, 7.5, 10, 12, and 15 min after injection and further processed for chromatographic analyses, as described above.

The blood samples (2 mL) were collected into heparinized tubes containing 7.3 mmol/L of iso-OMPA, a selective inhibitor of BuChE (*17*), to avoid in vitro hydrolysis of ^{11}C-MP4B. Plasma was obtained by centrifugation at 2,118*g* for 5 min at 4°C. For radio-HPLC analysis, the plasma proteins were precipitated with 10% 5-sulfosalicylic acid (1:1 v/v). The supernatant obtained after centrifugation (3,370*g* for 3 min at room temperature [RT]) was further filtered through a 0.45-μm PVDF Acrodisc filter (Gelman). For radio-TLC analysis, the plasma proteins were precipitated with 100% ethanol (1:1.5 v/v) followed by centrifugation (3,370*g* for 3 min at RT).

Radio-HPLC

The radio-HPLC system consisted of LaChrom (Merck Hitachi) pump L-7100, ultraviolet detector L-7400, and interface D-7000; a

radioisotope detector (Radiomatic 150TR; flow scintillation analyzer; Packard); and a computerized data acquisition system. Radio-HPLC was performed on an Ultracarb 7μ ODS(19) column (length, 250 mm; internal diameter, 10 mm; Phenomenex). The column was eluted using a gradient of methanol in aqueous 0.1 mol/L sodium-acetate, 0.1 mol/L citric acid, 1 mmol/L EDTA, and 5 mmol/L sodium heptane-sulfonate, 6 mL/min. After analyzing all plasma samples, an authentic standard containing ^{11}C-MP4B and its ^{11}C-labeled metabolite was run on radio-HPLC. The ^{11}C-labeled hydrolysis product was prepared in vitro from ^{11}C-MP4B in a reaction catalyzed by BuChE; 10 μL of BuChE (0.05 units/μL) were mixed with 200 μL of ^{11}C-MP4B, incubated for 1 min at RT and analyzed by radio-HPLC. The peaks of radioactivity were integrated with PC, and compounds in samples were identified by comparing the retention times of ^{11}C-MP4B and its labeled metabolite. The k′ values of ^{11}C-MP4B and the metabolite ^{11}C-MP4OH were 2.0 and 0.3, respectively, in the radio-HPLC analysis.

Radio-TLC

For comparison, plasma supernatants were separated using radio-TLC. Samples were applied on a Silicagel 60 F_{254} plate (Merck) using a Linomat IV applicator (Camag) connected to argon gas and developed with a mixture of ethyl acetate–isopropanol–ammonia (15:5:1 v/v/v) for 10 min (*12*). The TLC plate was briefly air dried and placed in a cassette in contact with a phosphor imaging plate (BAS-IP MP2025; Fuji Photo Film Co, Ltd.). The exposure time was 60 min. The distribution of radioactivity on the plate corresponding to unchanged ^{11}C-MP4B and its hydrolysis product was visualized and quantified using BAS-5000 phosphor imaging system (Fuji Medical Systems) and analyzed using Tina 2.0 software (Raytest Isotopenmessgeräte GmbH). The identification of compounds in blood plasma was based on the comparison of the retardation factor (R_f) values of authentic standards—^{11}C-MP4B, MP4B, and its hydrolysis product MP4OH—which were detected by radioactivity or by exposure to iodine vapor.

Kinetics of ^{11}C-MP4B in Human Blood

The comparison of plasma and metabolite kinetics (time course of total radioactivity and metabolite-corrected radioactivity in arterial plasma) of intravenously administered ^{11}C-MP4B between AD patients and healthy subjects was done by calculating the corresponding half-life ($t_{1/2}$/min) for each subject. The differences between the 2 groups was assessed using a 2-tailed *t* test, and statistical significance was inferred at $P < 0.05$.

Red Blood Cell Binding and Protein Binding of ^{11}C-MP4B

The ratio of radioactivity concentration in red blood cells versus plasma was determined in one healthy subject. Twenty blood samples were obtained from 0 to 50 min after intravenous injection of ^{11}C-MP4B. Whole blood was centrifuged at 2,118*g* for 5 min at 4°C to separate plasma and red blood cells. Aliquots (0.7 mL) of plasma and red blood cell fractions were obtained, and the radioactivity were measured with an automatic γ-counter (1480 Wizard 3″; EG&G Wallac). Subsequently, plasma proteins were precipitated with 10% 5-sulfosalicylic acid (1:1 v/v), centrifuged at 3,370*g* for 3 min at RT, and the radioactivity in supernatant and sediment was measured using a well-type γ-counter (7.62 × 7.62 cm [3 × 3 in]; Bicron). The percentage of radioactivity bound to plasma proteins was calculated thereafter.

A fixed amount of ^{11}C-MP4B was mixed with increasing concentrations of human albumin (fatty acid–free serum albumin; Sigma Chemical) and incubated at 37°C for 1 h in phosphate-buffered saline containing 10 mmol/L EDTA and 0.005% polysorbate 80. After the incubation, the samples were loaded onto Microcon YM-30 filters (regenerated cellulose membranes with a nominal molecular weight limit of 30,000; Millipore) and centrifuged at 9,500*g* for 10 min at RT. Radioactivity was measured from both the filtrate and the unfiltered solutions using a γ-counter (1480 Wizard 3″, EG&G Wallac). The amount of ^{11}C-MP4B bound to albumin was calculated by subtracting the amount of the unbound (filtrate).

RESULTS

Preparation of ^{11}C-MP4B

The radiopharmaceutical ^{11}C-MP4B was obtained in high radiochemical yields, 5–7 GBq, using a 40-min target irradiation with 17-MeV protons at 10 μA. The specific radioactivity was higher than 37 GBq/μmol at the end of a 27- to 33-min synthesis. Radiochemical purity was higher than 99%, and the tracer was radiochemically stable for more than 90 min.

Whole-Body Distribution of ^{11}C-MP4B

The whole-body PET images of a healthy male volunteer show that most of the radioactivity is distributed in the urinary bladder, indicating prompt excretion through the renal system. Renal pelvis, stomach, salivary glands, liver, kidneys, spleen, and vertebral column were also clearly visualized. However, the uptake in myocardium, pancreas, and lungs was low (Fig. 1). The average, SD, minimum, and maximum SUV values for the main organs are shown in Table 1. As much as 37% of the injected dose was excreted to urine voided immediately after PET, that is within 50 min after the tracer administration.

In Vivo Distribution and Biokinetics of ^{11}C-MP4B in Human Brain

In the brains of AD patients, ^{11}C-MP4B activity was highest in the cerebellum, followed by striatum, pons, and thalamus. Lower ^{11}C-MP4B activity was seen in cortical areas. Representative ^{11}C-MP4B PET images of the brain of an AD patient; the time–radioactivity curves for cerebellum, striatum, and cortex; and the corresponding total and metabolite-corrected radioactivity curves of the arterial plasma are shown in Figure 2. The ^{11}C-MP4B exhibits high initial uptake followed by gradual decrease. Approximately 30 min after the injection, the amount of radioactivity reaches a plateau in cerebellum, striatum, and cortex.

Separation of ^{11}C-MP4B from Its Radioactive Metabolite

Under the HPLC conditions described above, the retention times of ^{11}C-MP4B and its hydrolysis product were 7.1 ± 0.2 min (mean ± SD; range, 5.9–8.9 min) and 2.8 ±

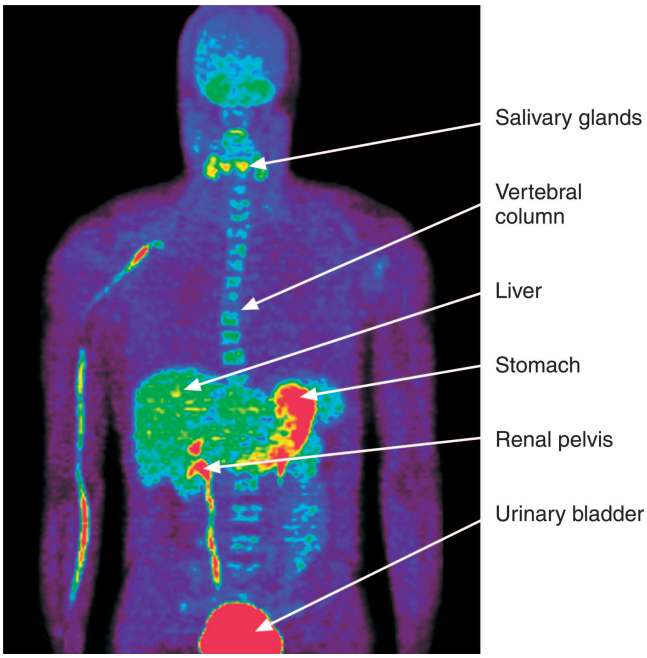

FIGURE 1. Whole-body PET images of 22-y-old man, showing distribution of intravenously administered ^{11}C-MP4B. Accumulation of tracer is clearly visible in urinary bladder, renal pelvis, stomach, liver, vertebral column, and salivary glands (arrows).

0.2 min (range, 2.6–3.0 min), respectively. A typical radio-HPLC chromatogram is shown in Figure 3A. Using the TLC method, the R_f values for ^{11}C-MP4B and its blood metabolite were 0.67 ± 0.04 (range, 0.57–0.73) and 0.56 ± 0.06 (range, 0.43–0.65), respectively. A representative TLC plate after separation and radiodetection is shown in Figure 3B.

Time Course of ^{11}C-MP4B in Human Plasma

Arterial blood samples were collected from 28 subjects during the ^{11}C-MP4B PET. For the purposes of metabolite analysis, plasma was isolated, deproteinized, and chromatographically analyzed. The peaks of radioactivity were integrated with a computer and decay corrected to the start of the analysis. The chemical identity was determined by comparing retention times (HPLC) or R_f values (TLC) with authentic standards.

The time course of ^{11}C-MP4B in human arterial plasma obtained by using radio-HPLC, radio-TLC, and combined results of radio-HPLC and radio-TLC are shown in Figures 4A, 4B, and 4C, respectively. A triexponential function was fitted to the mean values of ^{11}C-MP4B. The percentage of ^{11}C-MP4B declined rapidly. According to the radio-TLC analysis, the mean (±SD) values (n = 28) of ^{11}C-MP4B were 32% ± 14%, 29% ± 15%, 27% ± 14%, 22% ± 13%, 16% ± 11%, 11% ± 9%, 8% ± 7%, 7% ± 6%, and 7% ± 7% at 0.5, 1, 1.5, 3, 5, 7.5, 10, 12, and 15 min, respectively, after injection. According to the radio-HPLC analysis of the same samples, the percentages of unchanged ^{11}C-MP4B were 25% ± 14%, 22% ± 13%, 20% ± 13%, 15% ± 12%, 12% ± 9%, 6% ± 6%, and 6% ± 4% at 0.5, 1, 1.5, 3, 5, 10, and 15 min, respectively, after injection. When the results of both radio-HPLC and radio-TLC were combined, the values of unmetabolized ^{11}C-MP4B were 28% ± 14%, 23% ± 14%, 23% ± 14%, 18% ± 12%, 14% ± 10%, 11% ± 9%, 7% ± 6%, 7% ± 6%, and 6% ± 6% at 0.5, 1, 1.5, 3, 5, 7.5, 10, 12, and 15 min, respectively, after injection.

The time course of total radioactivity and metabolite-corrected radioactivity in arterial plasma was compared between AD patients and healthy subjects. The mean $t_{1/2}$ of total plasma kinetics in patients with AD and normal subjects was 1.65 ± 0.73 min and 1.40 ± 0.52 min, respectively. The mean of $t_{1/2}$ of metabolite-corrected plasma kinetics in patients with AD and normal subjects was 5.03 ± 2.19 min and 3.95 ± 1.18 min, respectively. However, the differences between groups did not reach statistical significance; P values were 0.28 and 0.18.

Protein Binding and Distribution of ^{11}C-MP4B in Human Blood

After intravenous injection of ^{11}C-MP4B into the study subjects, radioactivity cleared rapidly from blood and plasma. The blood-to-plasma ratio of radioactivity was about 1.0 and did not change appreciably over the 60-min duration of the PET imaging. Approximately 17% of ^{11}C-MP4B radioactivity was bound to human plasma proteins.

The binding of ^{11}C-MP4B to human albumin protein was studied in vitro using the ultrafiltration method. The ^{11}C-MP4B binding to albumin was concentration dependent. Under physiologic concentration (albumin concentration in human plasma is 35–50 g/L [550–750 μmol/L]), approximately 20% of ^{11}C-MP4B was bound to albumin (Fig. 5).

DISCUSSION

^{11}C-MP4B, a substrate for BuChE, is a promising new tracer for the in vivo evaluation of BuChE activity using PET. This study describes for the first time the whole-body distribution and the metabolic fate of intravenously admin-

TABLE 1
SUV For Main Organs in Whole-Body ^{11}C-MP4B PET

Organ	SUV (g/mL)			
	Mean	SD	Min	Max
Urinary bladder	9.02	0.97	7.04	10.37
Renal pelvis	8.27	3.69	2.76	13.41
Stomach	6.83	1.10	4.18	8.51
Salivary gland	3.34	0.54	2.29	4.17
Liver	2.68	0.36	2.07	3.49
Kidney	2.43	0.44	1.51	3.11
Spleen	2.17	0.26	1.84	2.84
Vertebral column	2.13	0.31	1.52	2.66
Brain	1.82	0.48	0.63	3.28

Min = minimum; Max = maximum.

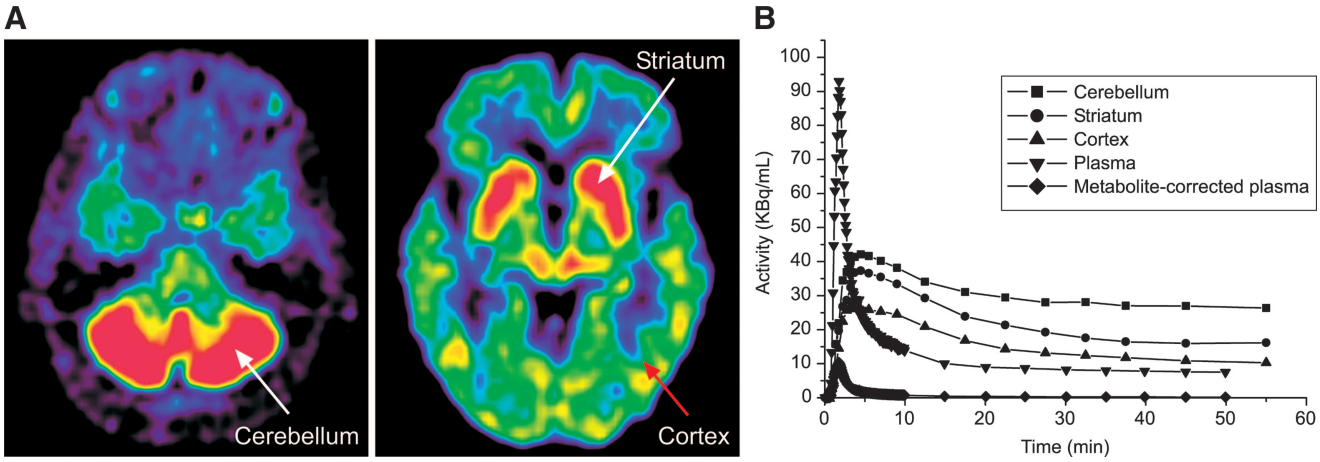

FIGURE 2. (A) PET images showing radioactivity distribution in brain of AD patient (70-y-old man) after 731-MBq intravenous injection of ^{11}C-MP4B. Images are summated from 20 to 40 min after injection and color coded according to amount of radioactivity, from dark blue (lowest) to hot red (highest). (B) Time-radioactivity curves for cerebellum, striatum, and cortex and corresponding total and metabolite-corrected radioactivity curves of arterial plasma.

istered ^{11}C-MP4B in humans. Our results reveal that ^{11}C-MP4B is cleared very rapidly from blood and is rapidly excreted through the renal system. Furthermore, metabolite analysis showed a dramatic metabolization of ^{11}C-MP4B in blood circulation.

Regarding the preparation of ^{11}C-MP4B, some precautions were observed. To prevent radiolysis, sterile propylene glycol–ethanol (7:3 v/v) was added to the HPLC-purified product before evaporation. Since the free base of the product, ^{11}C-MP4B, is volatile at reduced pressure, a small amount of hydrochloric acid was added to the HPLC-purified product before evaporation to convert it into a hydrochloride salt, which is not volatile. It has been reported that the addition of hydrochloric acid before the evaporation of

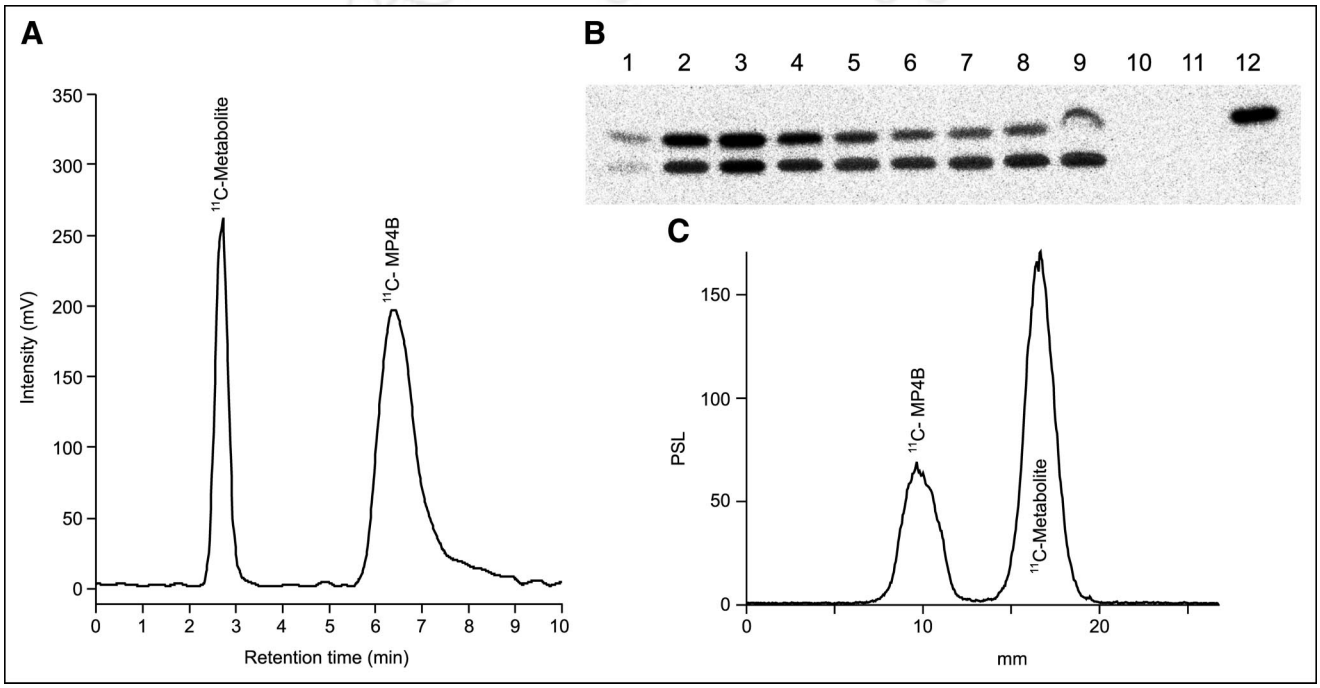

FIGURE 3. (A) Representative radio-HPLC chromatogram of an arterial plasma sample showing 2 peaks identified as metabolite and intact ^{11}C-MP4B. Retention times for peaks were 2.85 and 6.51 min, respectively. (B) Radioactivity in TLC plate of arterial plasma samples taken 0.5–15 min after injection (lanes 1–9). Spots for ^{11}C-MP4B (a, $R_f = 0.69$) and its metabolite (b, $R_f = 0.51$) were clearly visible in each sample. Lanes 10, 11, and 12 correspond to authentic standards: MP4B, MP4OH, and ^{11}C-MP4B, respectively. The nonradioactive compounds were visualized afterwards by exposure to iodine vapor. (C) Representative chromatogram of lane 7.

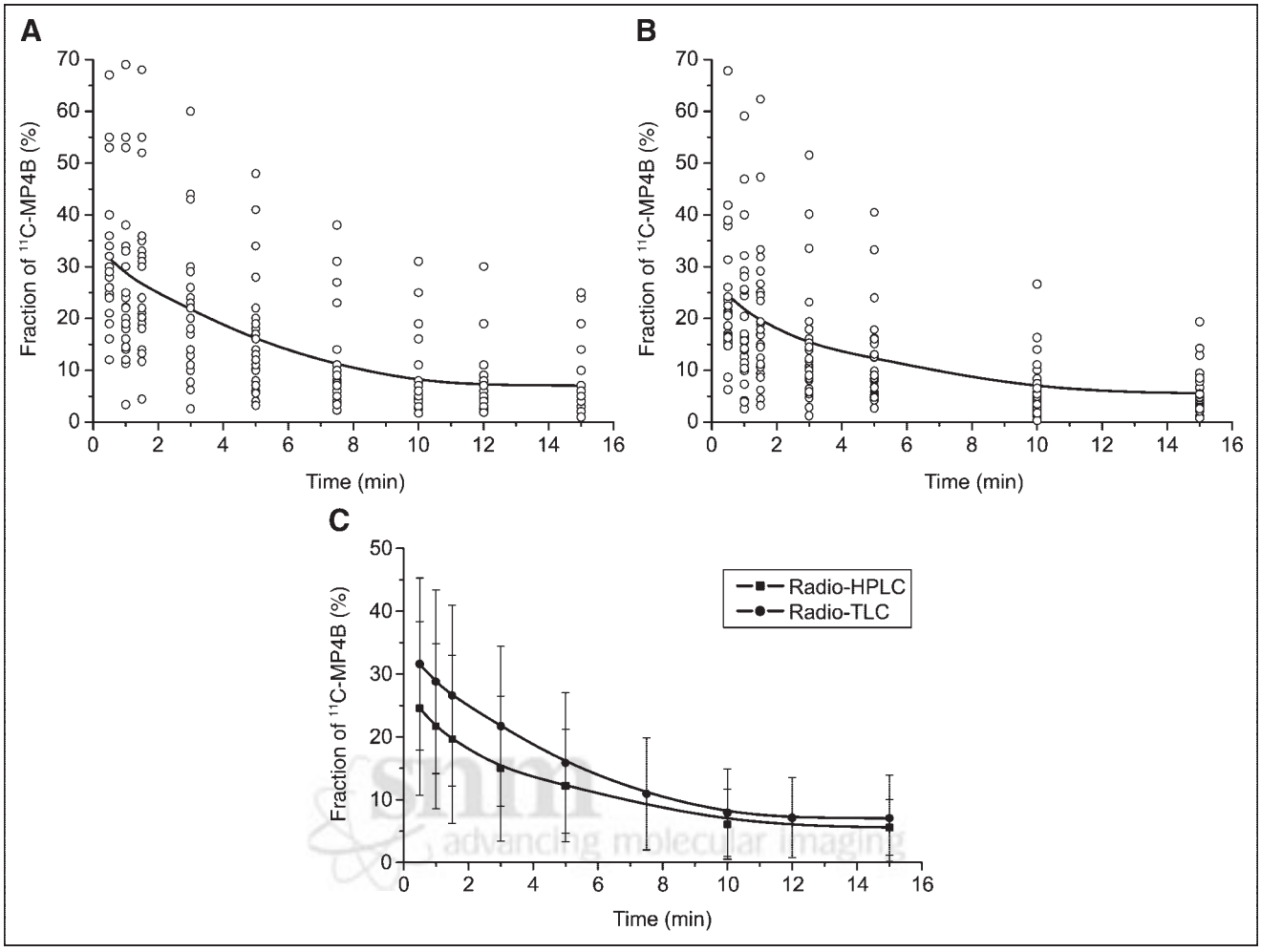

FIGURE 4. Concentration (%) of ^{11}C-MP4B in human arterial plasma during PET as a function of time. Results are from 28 subjects for radio-HPLC (A), radio-TLC (B), and combined results of radio-HPLC and radio-TLC (C). Individual results (○), triexponential curve fit (lines), and SD (columns) are shown.

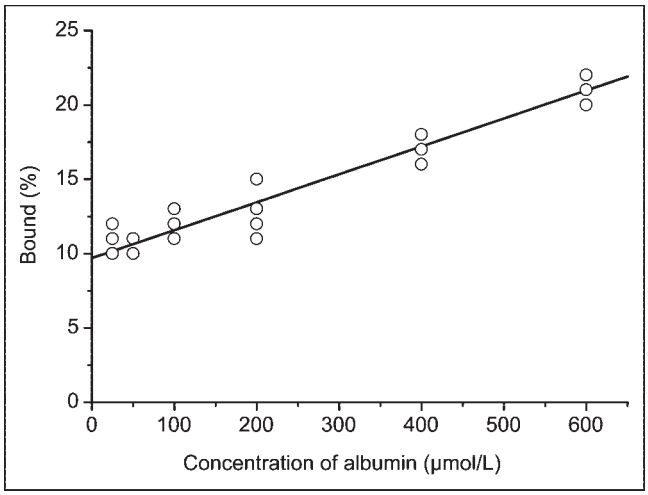

FIGURE 5. Albumin binding of ^{11}C-MP4B determined in vitro. Line represents mean values of experiments (n = 3).

a structurally similar radiopharmaceutical, ^{11}C-PMP or ^{11}C-MP4P, led to significant product degradation (*18*). We did not experience any significant product degradation during evaporation, which suggests that the degradation reported by Snyder et al. (*18*) was not due to acidic decomposition, but rather to radiolysis, which in our method was efficiently suppressed by the addition of propylene glycol–ethanol before evaporation. In recent reports on the production of another ^{11}C-MP4B analog, ^{11}C-MP4A, the acidification with hydrochloric acid before evaporation did not lead to significant product degradation either (*6,9*).

Since ^{11}C-MP4B is excreted in the urine, the bladder and urinary tract showed intense activity; thus, they are the critical organs. The radiation burden to the urinary wall can be reduced by maximizing the initial bladder content volume at the time of injection. Uptake in the stomach and in salivary glands reflects accumulation in mucosa in general. Furthermore, the clear uptake in vertebral column may indicate bone marrow involvement. For accurate radiation

dosimetry of ^{11}C-MP4B PET, the effective dose of the critical organs should be defined.

In general, to develop a biomathematic model to interpret the kinetics of radioactivity uptake in the target tissue, it is crucial to understand the metabolism of the new imaging agent. Quantifying metabolic processes with dynamic PET and tracer kinetic modeling relies on the time course of intact tracer in plasma, that is, the input curve. Careful validation of the quantification procedure, that is, the fractional rate of ^{11}C-MP4B hydrolysis, is necessary because PET is a single-signal technique, and the in vivo–formed radioactive metabolites might contribute to the signal, thus disturbing data analysis. In the present study, analysis of ^{11}C-MP4B metabolites in plasma was performed during the PET examination with ^{11}C-MP4B in 28 human subjects (58–80 y of age), including 18 healthy volunteers and 10 patients with AD. Arterial plasma samples were obtained at 0.5–15 min after intravenous injection of the tracer and were analyzed by radio-HPLC and radio-TLC. Human plasma contains approximately 8 ng/mL of AChE and 3,300 ng/mL of BuChE (*19*); therefore, inhibition of in vitro hydrolysis of ^{11}C-MP4B was required. The concentration of iso-OMPA used in this study was 7.3 mmol/L, which has been shown in our laboratory to be sufficient (data not shown). It was found that intravenously injected ^{11}C-MP4B is rapidly hydrolyzed in blood circulation. Thus, as soon as 15 min after the injection, the parent tracer represented only 6% of the total radioactivity in plasma. Although large individual variation was observed in the rate of plasma ^{11}C-MP4B hydrolysis, no significant differences were found either between men and women or between normal subjects and patients. When the mean fraction of unchanged ^{11}C-MP4B at each time point was used, instead of individually measured metabolite data, for the arterial input function, as high an error as 31% ± 14% (range, 6%–68%) occurred in the k_3 value of the ^{11}C-MP4B, representing BuChE activity in the brain. These results indicate that the mean percentage of unchanged ^{11}C-MP4B fraction in subjects cannot be used as the standardized value and that the analysis of metabolites in plasma is necessary to determine the exact arterial input function for quantitative PET measurement.

In the case of ^{11}C-labeled compounds, the radio-HPLC is often the most appropriate technique for plasma radioactive metabolite analysis (*20*). However, the described radio-TLC method for the separation of ^{11}C-MP4B and its hydrolysis product was more sensitive than the radio-HPLC method, which is of importance when it comes to the analysis of samples with low radioactivity. The radioactivity in circulating blood decreased rapidly after intravenous injection of ^{11}C-MP4B; consequently, the radio-TLC was a more convenient method in the respect that all radioactivity applied on the plate can be accounted for and quantified. The radio-TLC method using ethyl acetate–isopropanol–ammonia yielded better separation between ^{11}C-MP4B and ^{11}C-MP4OH than the method using dichloromethane–methanol–ammonia as described by Snyder et al. (*16*). Since ^{11}C has a short half-life of 20.4 min, the amounts of ^{11}C-MP4B and the metabolite, ^{11}C-MP4OH, in plasma at 20–60 min after injection could not be determined reliably using either radio-TLC or radio-HPLC but had to be estimated by extrapolation.

Although the PET brain activity measurements are not the main topic of this paper, we have provided some results for brain distribution (Fig. 1). In brains of patients with AD, ^{11}C-MP4B activity was the highest in cerebellum, followed successively by striatum, pons, and thalamus. The cortical areas exhibited lower activity. The biodistribution of ^{11}C-MP4B in brains of patients with AD are in accordance with the neuroanatomy of BuChE seen in postmortem studies of human brain, except the observed much higher uptake in striatum than in cortex (*21*). Further studies with larger number of AD patients to better characterize the value of ^{11}C-MP4B PET for the evaluation of cerebral BuChE activity are in progress. These studies will include calculations of regional kinetic parameters; for example, to clarify whether the cholinesterase treatment affects ^{11}C-MP4B uptake in human brain.

CONCLUSION

Our study suggests that although ^{11}C-MP4B PET may provide information on in vivo activity of BuChE, careful metabolite analysis of plasma is essential to determine the exact arterial input function for quantitative PET measurements. In addition, subsequent prospective studies for the radiation dosimetry of ^{11}C-MP4B PET are suggested.

ACKNOWLEDGMENTS

The authors thank the staff of the Turku PET Centre. This study was supported by the Turku University Hospital and the Päivikki and Sakari Sohlberg Foundation.

REFERENCES

1. Perry E, McKeith I, Ballard C. BuChE and progression of cognitive deficits in dementia with Lewy bodies. *Neurology.* 2003;60:1852–1853.
2. Mesulam MM, Geula C. Butyrylcholinesterase reactivity differentiates the amyloid plaques of aging from those of dementia. *Ann Neurol.* 1994;36:722–727.
3. Perry EK, Perry RH, Blessed G, Tomlinson BE. Changes in brain cholinesterases in senile dementia of Alzheimer type. *Neuropath Appl Neurobiol.* 1978;4:273–277.
4. Ballard CG. Advances in the treatment of Alzheimer's disease: benefits of dual cholinesterase inhibition. *Eur Neurol.* 2002;47:64–70.
5. Moran MA, Mufson EJ, Gomez-Ramos P. Cholinesterases colocalize with sites of neurofibrillary degeneration in aged and Alzheimer's brains. *Acta Neuropathol.* 1994;87:284–292.
6. Kaasinen V, Någren K, Järvenpää T, et al. Regional effects of donepezil and rivastigmine on cortical acetylcholinesterase activity in Alzheimer's disease. *J Clin Psychopharm.* 2002;22:615–620.
7. Namba H, Fukushi K, Nagatsuka S, et al. Positron emission tomography: quantitative measurement of brain acetylcholinesterase activity using radiolabeled substrates. *Methods.* 2002;27:242–250.
8. Kuhl DE, Minoshima S, Frey KA, Foster NL, Kilbourn MR, Koeppe RA. Limited donepezil inhibition of acetylcholinesterase measured with positron emission tomography in living Alzheimer cerebral cortex. *Ann Neurol.* 2000;48:391–395.

9. Herholz K, Bauer B, Wienhard K, et al. In-vivo measurements of regional acetylcholine esterase activity in degenerative dementia: comparison with blood flow and glucose metabolism. *J Neural Transm.* 2000;107:1457–1468.
10. Irie T, Fukushi K, Akimoto Y, Tamagami H, Nozaki T. Design and evaluation of radioactive acetylcholine analogs for mapping brain acetylcholinesterase (AChE) in vivo. *Nucl Med Biol.* 1994;21:801–808.
11. Kilbourn MR, Snyder SE, Sherman PS, Kuhl DE. In vivo studies of acetylcholinesterase activity using a labeled substrate, N-[^{11}C]methylpiperdin-4-yl propionate ([^{11}C]PMP). *Synapse.* 1996;22:123–131.
12. Irie T, Fukushi K, Namba H, et al. Brain acetylcholinesterase activity: validation of a PET tracer in a rat model of Alzheimer's disease. *J Nucl Med.* 1996;37: 649–655.
13. Tanaka N, Fukushi K, Shinotoh H, et al. Positron emission tomographic measurement of brain acetylcholinesterase activity using N-[(11)C]methylpiperidin-4-yl acetate without arterial blood sampling: methodology of shape analysis and its diagnostic power for Alzheimer's disease. *J Cereb Blood Flow Metab.* 2001;21:295–306.
14. Kuhl DE, Minoshima S, Frey KA, Foster NL, Kilbourn MR, Koeppe RA. Limited donepezil inhibition of acetylcholinesterase measured with positron emission tomography in living Alzheimer cerebral cortex. *Ann Neurol.* 2000;48:391–395.
15. Herholz K, Weisenbach S, Zundorf G, et al. In vivo study of acetylcholine esterase in basal forebrain, amygdala, and cortex in mild to moderate Alzheimer disease. *Neuroimage.* 2004;21:136–143.
16. Snyder SE, Gunupudi N, Sherman PS, et al. Radiolabeled cholinesterase substrates: in vitro methods for determining structure-activity relationships and identification of a positron emission tomography radiopharmaceutical for in vivo measurement of butyrylcholinesterase activity. *J Cereb Blood Flow Metab.* 2001;21:132–143.
17. Koelle GB, Davis R, Diliberto EJ Jr, Koelle WA. Selective, near-total, irreversible inactivation of peripheral pseudocholinesterase and acetylcholinesterase in cats in vivo. *Biochem Pharmacol.* 1974;23:175–188.
18. Snyder SE, Tluczek L, Jewett DM, Nguyen TB, Kuhl DE, Kilbourn MR. Synthesis of 1-[^{11}C]methylpiperidin-4-yl propionate ([^{11}C]PMP) for in vivo measurements of acetylcholinergic activity. *Nucl Med Biol.* 1998;25:751–754.
19. Brimijoin S, Hammond P. Butyrylcholinesterase in human brain and acetylcholinesterase in human plasma: trace enzymes measured by two-site immunoassay. *J Neurochem.* 1988;51:1227–1231.
20. Stöcklin G, Pike VW. *Radiopharmaceuticals for Positron Emission Tomography: Methodological Aspects.* Dordrecht, The Netherlands: Kluwer Academic Publishers; 1993:151–178.
21. Mesulam M. Neuroanatomy of cholinesterases in the normal human brain and in Alzheimer's disease. In: Ciacobini E, ed. *Cholinesterases and Cholinesterase Inhibitors.* London, U.K.: Martin Dunitz; 2000:121–137.